ELSEVIER

Journal of Electrostatics 42 (1997) 69-81

Journal of
ELECTROSTATICS

# Electrostatic Effects in Micromachined Actuators for Adaptive Optics

Mark N. Horenstein[a], Thomas G. Bifano[b], Raji Krishnamoorthy Mali[b], and Nelsimar Vandelli[b]

[a]Department of Electrical and Computer Engineering, Boston University, 44 Cummington St., Boston, MA 02215, mnh@bu.edu

[b]Department of Aerospace and Mechanical Engineering, Boston University, 44 Cummington St., Boston, MA 02215, tgb@bu.edu

ABSTRACT

The electrostatic properties of double-cantilevered micro-electromechanical silicon actuators are examined for possible use in large-scale, deformable mirror arrays. Devices display typical nonlinear deflection versus voltage characteristics and electromechanical instability at elevated voltages. When the polysilicon membrane is suspended over a substrate with an insulating layer, the effects of electrostatic charge migration and contact charging alter actuator performance.

## 1. INTRODUCTION

Over the past several years, much progress has been made in the development of micron-sized mechanical devices made on silicon wafers. The fabrication of micromachined electromechanical systems, or MEMS, uses the same photolithography and etching techniques from which electronic integrated circuits are made. MEMS devices have small air gaps and small geometrical size, and thus can sustain relatively large electric fields without breakdown. The electrostatic forces produced by these large fields are comparable to the counteracting mechanical forces present in devices of small size, making electrostatic control of motion and position possible. MEMS is quickly becoming a mature technology, and many researchers have reported success in building electrostatic motors, actuators, transducers, and other devices using MEMS techniques.

One promising application for MEMS devices is in the area of adaptive optics. In many optical systems, image resolution and clarity can be greatly improved by using mirrors whose surfaces can be distorted by distances on the order of an optical wavelength. Such intentional

This work was supported by the U.S. Defense Advanced Research Projects Administration (DARPA) under Grant No. DABT 63-95-C-0065.

0304-3886/97/$17.00 © Elsevier Science B.V. All rights reserved.
*PII* S0304-3886(97)00138-1

surface distortion can compensate for unwanted wavefront distortion caused by noisy optical signal paths. One common cause of wavefront distortion, for example, is the random change in the refractive index of air due to thermal currents. The system depicted in Fig. 1 illustrates one possible scenario in which a flexible mirror compensates for the random changes in ray direction caused by the distorting medium. Without the adaptive mirror, the image would appear blurred to the camera. The flexible mirror surface is instead shaped so as to straighten out the distorted rays.

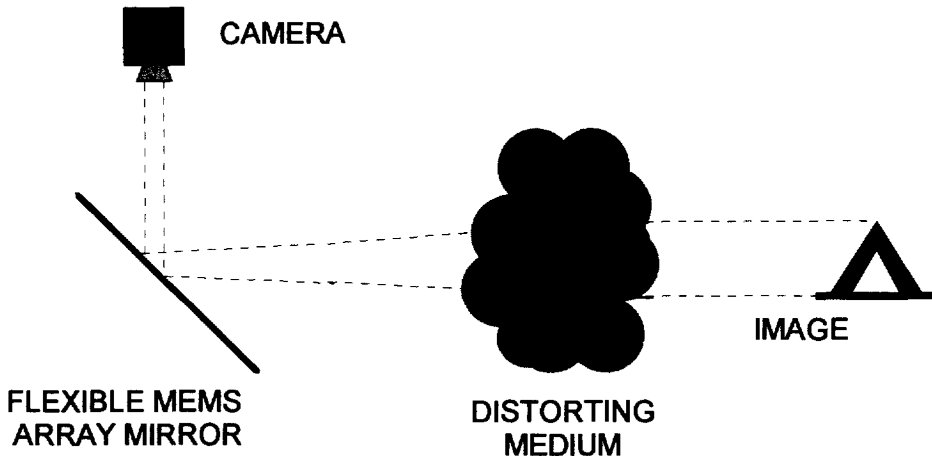


Figure 1 - Flexible MEMS array mirror compensates for distortion in the optical path.

The eventual goal of our research is the creation of an adaptive optic mirror consisting of a flexible diaphragm supported by an array of electrostatically-actuated double-cantilevered MEMS devices. Applying appropriate voltages to the actuators under real time control will cause intentional voltage-dependent distortions in the mirror surface resulting in corrections to the optical signal path. A simplified diagram of a typical mirror structure is shown in Fig. 2. Each actuator cell is activated by a separate analog voltage and deflects downward toward the substrate plane when voltage is applied. In the top figure, voltage is applied to no cells, leaving all actuators at rest and the mirror surface flat. In the lower figure, actuators are energized to varying voltages, causing varying point-by-point deflection and predictable distortion of the mirror surface.

## 2. BASIC ACTUATOR DEVICE

The ultimate feasibility test of MEMS-based adaptive optics will be their successful integration into large scale systems. Such a task requires individual actuators that are robust, easy to make, and highly reliable. Devices must also have repeatable deflection versus voltage characteristics. Despite the importance of large scale system issues, an understanding of the properties of each individual cell is also extremely important. This paper focuses on several of the electrostatic properties and deflection characteristics of individual MEMS actuators cells. All devices described were fabricated using the MCNC "MUMPS" process.

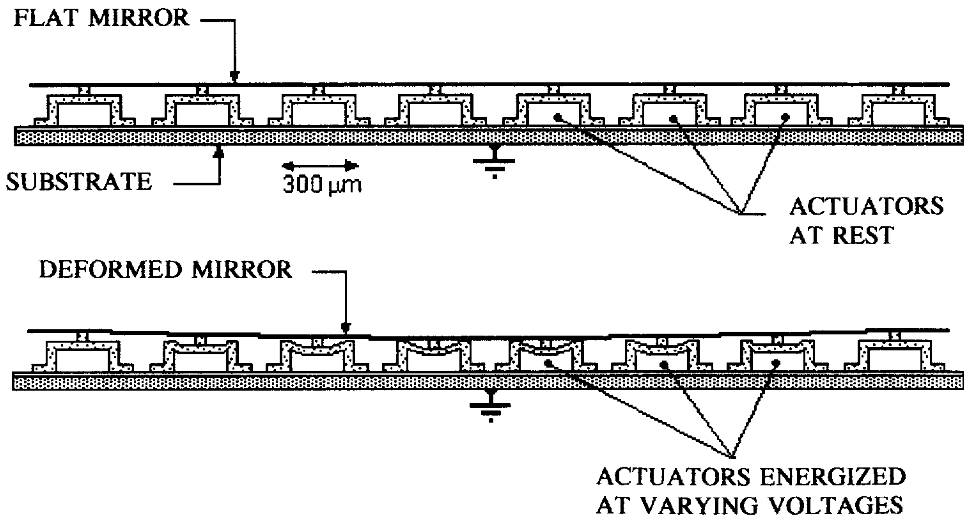


Figure 2 - Flexible mirror supported by an array of double-cantilevered MEMS cells.

The double cantilever device configurations of Figs. 3 and 4 are both possible candidates for future large-scale integration. The first device (not drawn to scale) consists of a 2-$\mu$m thick rectangular polysilicon membrane suspended by two rigid walls above a 0.5-$\mu$m thick insulating silicon-nitride layer that covers a silicon substrate. The gap between the membrane and the nitride layer is about 2 $\mu$m. The nitride layer is required to passivate the silicon substrate. Planar length and width dimensions of the device range from 100 to 300 $\mu$m. Contact pads permit electrical contact to the membrane by lithographed polysilicon wires or wire-bonded leads. Applying a voltage between the membrane and grounded substrate causes the membrane to deflect downward due to electrostatic forces, as shown in Fig. 5. The alternative device of Fig. 4 is of similar construction but includes an additional 0.5 $\mu$m-thick polysilicon electrode on top of the nitride layer. In this case, the voltage is applied between the membrane and the lower polysilicon electrode. The substrate may be left floating or grounded. For both devices, voltages on the order of 30 to 140 V, depending on the length of the suspended membrane, are required for the full range of deflection. These voltages represent field strengths in the range 15 to 70 V/$\mu$m in the air gap beneath the membrane. Note that the 2-$\mu$m gap spacing lies at the low end of the Paschen breakdown curve [1,2,3]. In air at atmospheric pressure, a 2 $\mu$m gap can support electric fields as high as about 70 V/$\mu$m, corresponding to actuator voltages of up to 140 V.

The structure of Fig. 3 has the advantage that a complete collapse of the membrane to the nitride surface due to accidental overvoltage will not short out the driving electronics. Without this feature, the device might otherwise be destroyed due to excessive current flow and energy dissipation. The alternative of providing current limiting in the drive electronics is undesirable because it usually limits high speed performance, contrary to one important

requirement of a MEMS array designed for real time optical signal processing. Although the simple structure of Fig. 3 eliminates the short-circuit problem, it is susceptible to effects of charge migration and contact charging, as will be shown in a later section. The addition of the polysilicon electrode, as in the structure of Fig. 4, minimizes these undesirable electrostatic effects but requires extreme care in operation to prevent short circuits due to actuator overvoltage.

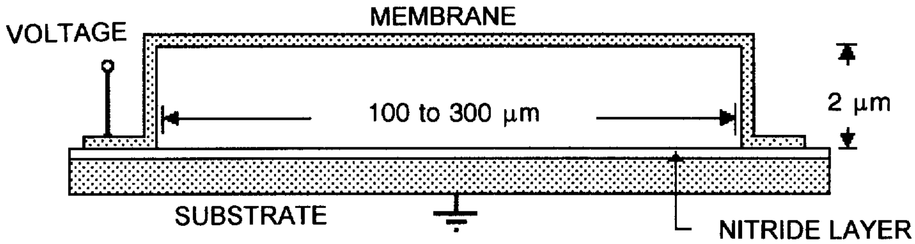


Figure 3 - Basic MEMS actuator device consisting of polysilicon diaphragm and nitride layer over silicon substrate. Contact pads connected to the membrane allow voltage to be applied.

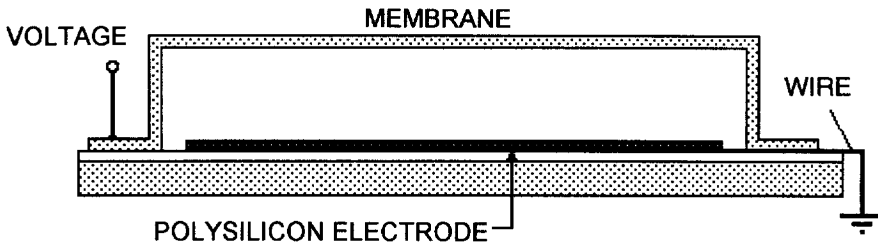


Figure 4 - MEMS actuator with additional polysilicon electrode placed on top of the nitride layer.

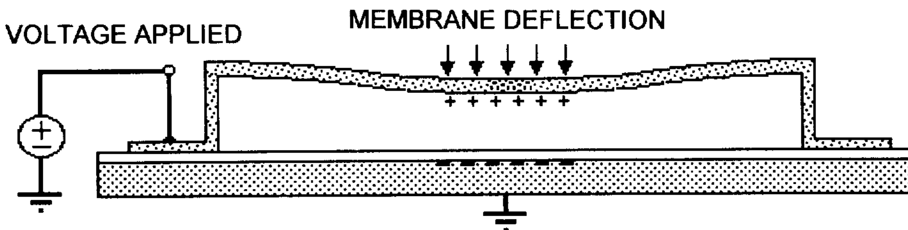


Figure 5 - Actuator membrane deflects toward the substrate when voltage is applied.

## 3. EXPERIMENTAL APPARATUS

Devices were tested using the apparatus shown in Fig. 6. Actuator deflection was monitored using a commercially available 0.63-$\mu$m HeNe laser doppler interferometer. Voltages between 0 and 120 V were applied using a digital-to-analog converter and voltage amplifier driven by a desktop computer. Although the actuators could have been driven directly from a voltage power supply in these simple experiments, a computer-based system was developed in anticipation of future large-scale arrays and the incorporation of such arrays into real time feedback control systems.

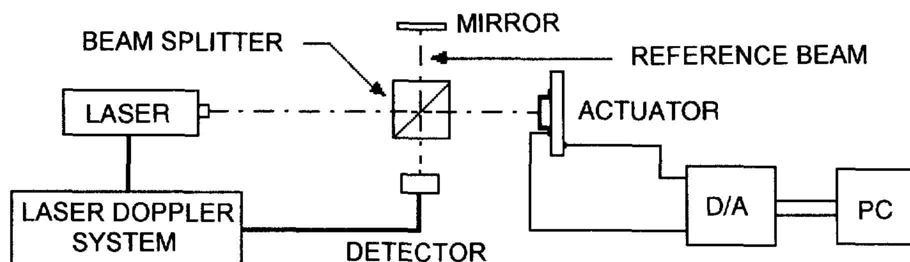


Figure 6 - Experimental apparatus used to measure membrane position versus voltage for individual actuators. Position is monitored using a commercial laser doppler-shift interferometer.

The curve marked "data" in Fig. 7 shows a plot of actuator deflection measured at the center of the membrane versus applied voltage. This curve was obtained for a 300 $\mu$m × 300 $\mu$m actuator using the system of Fig. 6. The plot exhibits features typical of a double cantilevered MEMS device. The deflection first increases slowly with voltage, then more rapidly until a point of instability, called "snap through", occurs. At the snap-through voltage, electric forces begin to increase more rapidly with deflection than do the restoring mechanical forces provided by the elastic membrane. Above the snap-through voltage, the actuator membrane collapses to the substrate. For our devices, the snap-through instability occurred for deflections exceeding about one-third of the total gap spacing.

## 4. A SIMPLE MODEL FOR ACTUATOR DEFLECTION

The fundamental features of the actuator deflection versus voltage curve can be easily understood using the overly simplified two-dimensional discretized model of Fig. 8, in which the actuator is represented by horizontal sections of membrane, each located at a different height relative to the substrate. Mechanical forces between segments are represented by linear springs; electric forces are modeled as those of simple parallel-plate capacitors. This simple model is essentially identical to that reported by previous authors [4,5] and can be used to understand qualitatively the snap-through feature of the deflection versus voltage curve. It requires that two simplifying assumptions be made. First, the lateral dimensions of the

membrane must be large compared to the gap spacing, so that the electric field beneath each section of the membrane will be nearly uniform with no fringing. Second, for small deflections the mechanical force on each segment must be proportional to its position relative to its nearest neighbors. Using this simple model, one can show that the observed electromechanical instability is fundamental to the geometry of the membrane and its planar orientation relative to the ground plane. The onset of instability can be predicted without knowledge of the specific mechanical properties of the bending membrane, although knowledge of the latter is required to achieve precise predictions of the deflection contour as a function of applied voltage.

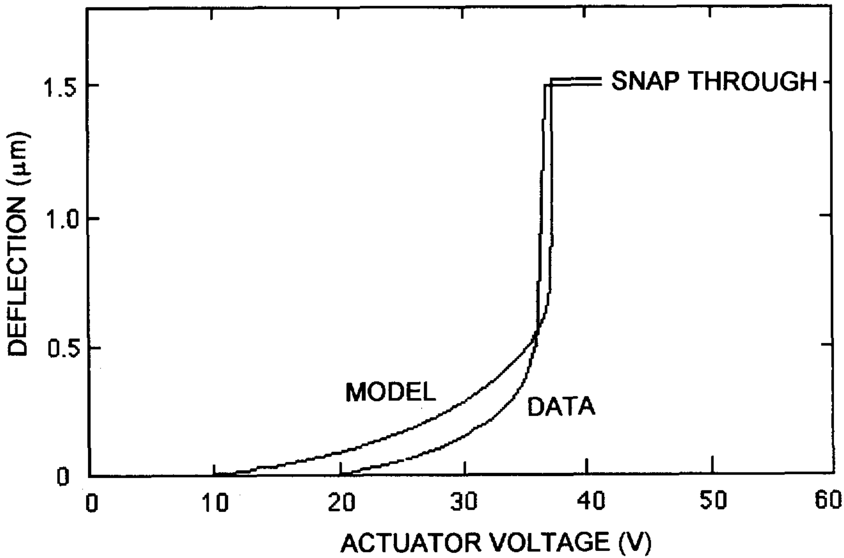


Figure 7 - DATA: Experimental deflection vs. voltage curve for a 300 $\mu$m × 300 $\mu$m actuator. MODEL: Curve predicted from a numerical solution of Eqs. (1) and (2).

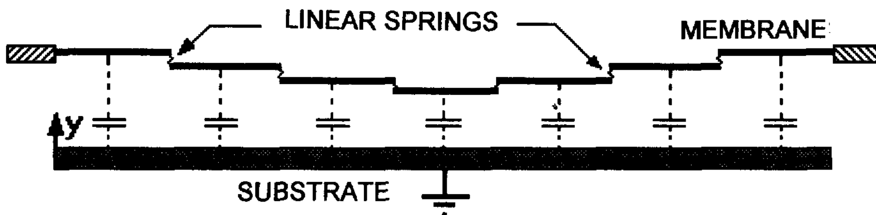


Figure 8 - Simple discretized model for predicting actuator performance. Mechanical forces are modeled as linear springs between nodes; electrical forces are computed from the derivative of the stored electrical energy on each discrete membrane segment.

For a given applied voltage $V$, the force of electrostatic origin on the $n$th segment of the membrane can be found by taking the derivative of its stored electrical energy:

$$F_{\text{elec-n}} = \frac{d}{dy}\frac{CV^2}{2} = \frac{V^2}{2}\frac{d}{dy}\frac{\epsilon A}{y_n} = -\frac{V^2}{2}\frac{\epsilon A}{y_n^2} \tag{1}$$

Here $y_n$ is the height of the segment above the substrate, $\epsilon$ the dielectric constant of the gap space, and $A$ the area of the segment. The mechanical force on the $n$th segment can be approximated by computing the height difference between the segment and its ($n$-1)th and ($n$+1)th neighbors:

$$F_{\text{mech-n}} = k\,(y_{n-1} - y_n) + k\,(y_{n+1} - y_n) \tag{2}$$

In this simple model, $k$ is a constant related to the membrane thickness, elastic modulus, and overall physical geometry. Equations (1) and (2) can be solved numerically by iteration to predict the membrane shape at which force equilibrium occurs for a given applied voltage, subject to the boundary conditions $y = g$ (where $g$ is the gap spacing) at the two supported edges. One such set of deflection curves, obtained over the voltage range 0 to 40 V using the parameters $k = 0.02$ N/m, $g = 2$ $\mu$m, $\epsilon = \epsilon_0$, and $A = 300$ $\mu$m $\times$ 300 $\mu$m, is shown in Fig. 9. The value of $k$ was chosen empirically to obtain a predicted snap-through voltage consistent with values of snap-through voltage observed experimentally. Plotting the vertical displacement at the membrane center versus applied voltage leads to the displacement/voltage curve labeled "model" in Fig. 7. The computed curve is compared in Fig. 7 to measured displacement data for an actual 300 $\mu$m $\times$ 300 $\mu$m device. As is evident in the figure, the very simple model of Fig. 8. predicts the overall shape of the curve as well as the onset of snap-through instability. More detailed analyses which account for the detailed mechanical characteristics of the bent-beam membrane as well as the field distortion due to its deflection also predict the snap-through instability but provide a much more accurate prediction of actuator deflection and membrane shape [5,6,7].

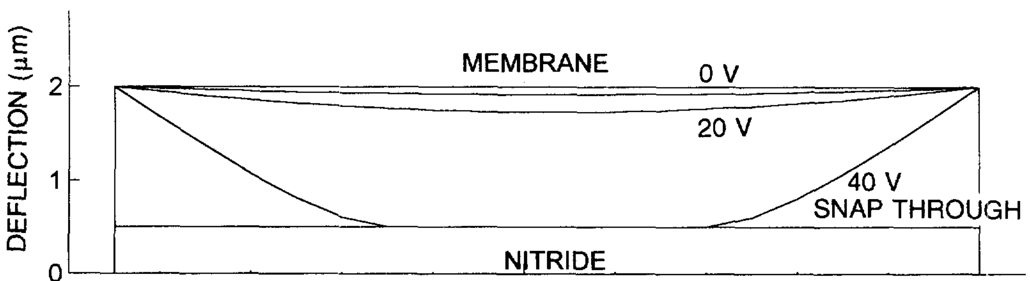


Figure 9 - Membrane deflection profiles at various applied voltages.

## 5. ELECTROSTATIC CHARGE MIGRATION EFFECT

When an actuator reaches snap through, its flexible membrane "bottoms out" on the underlying substrate. As previously mentioned, the insulating nitride layer covering the substrate in the device of Fig. 3 prevents internal short circuits, thereby enhancing system robustness. This same feature, however, can lead to a troublesome charge migration effect that we have observed on some actuators. The plot of Fig. 10 shows the measured deflection versus time for one such actuator. To obtain this plot, the actuator voltage was driven by a 1 Hz, 0 to 28-V square wave. The deflection was measured just after each rising transition. (Applying a square wave voltage having a net dc component, rather than pure dc, produces the observed charge migration effect but results in a superior signal-to-noise ratio in the laser-doppler interferometer measurement system.) An increase in deflection with time due to the dc component of the applied voltage is clearly evident. One possible explanation for this phenomenon can be understood by examining the actuator of Fig. 11. The top figure depicts the location of charge when the voltage is first applied. The one-dimensional uniform gap conditions become

$$E_1 d_1 + E_2 d_2 = V, \text{ and} \tag{3}$$

$$\epsilon_0 E_1 = \epsilon_2 E_2 \tag{4}$$

where $E_1$ and $E_2$ are the electric field magnitudes in regions 1 and 2, respectively. These one-dimensional field equations are only approximate in this case because the membrane is not really flat. Solving Eqs. (3) and (4) yields the electric field strength in the gap:

$$E_1 = \frac{V}{d_1 + (\epsilon_0/\epsilon_2)d_2} \tag{5}$$

Over time, charge will migrate to the exposed nitride surface. In our devices, charge migration is thought to occur over surface leakage paths, rather than through the bulk of the nitride. After complete charge relaxation has occurred and a steady state field condition has been reached, the actuator will appear as in the bottom portion of Fig. 11. In this case, $E_2$ is reduced to zero, and the field in the gap becomes simply $E_1{}^* = V/d_1$. Under these conditions, actuator deflection increases after charge migration because $E_1{}^*$ will be larger than $E_1$. The ratio of the two field values after and before charge migration becomes

$$\frac{E_1{}^*}{E_1} = \frac{d_1 + (\epsilon_0/\epsilon_2)d_2}{d_1} \tag{6}$$

This ratio can be used to predict the increase in deflection by assuming the effect of charge migration to be equivalent to an increase in applied voltage without charge migration. The voltage used to produce the deflection in the pre-charge migration plot of Fig. 10 was 28 V, yielding a pre-charge migration displacement of about 0.2 $\mu$m and a residual gap spacing $d_2$ of about 1.8 $\mu$m, as shown by the white circle in Fig. 12. For an estimated dielectric constant and thickness for the nitride layer of $\epsilon_2 = 3\epsilon_0$ and $d_2 = 0.5$ $\mu$m, respectively, the

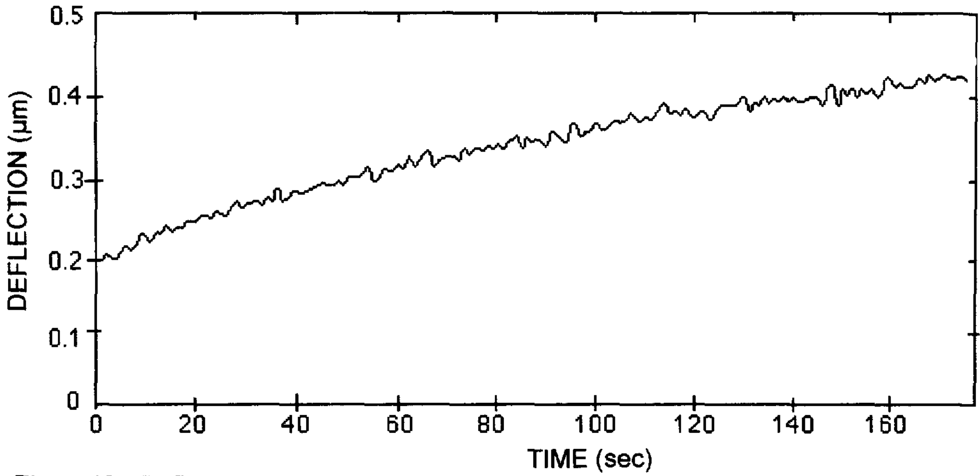


Figure 10 - Deflection versus time for an actuator of the type depicted in Fig. 3. A zero to 28-V, 1-Hz square-wave is applied.

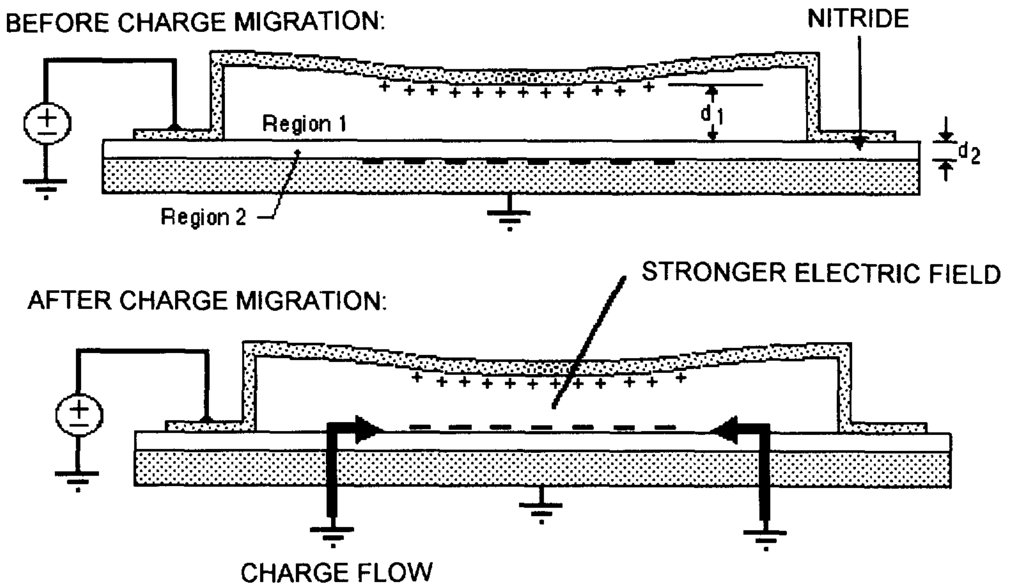


Figure 11 - Location of charge before and after charge migration. Charge flows to the top of the nitride layer over surface leakage paths.

field enhancement factor (6) after charge migration becomes about 1.1. We may thus project an "enhanced" voltage value of 28 V $\times$ 1.1 $\approx$ 31 V on the curve of Fig. 12 to predict the true deflection after charge migration. The black circle in Fig. 12 represents the equivalent voltage of 31 V yielding the extrapolated displacement of about 0.5 $\mu$m actually measured at the right-hand end of Fig. 10. Although the agreement is not perfect, the trend clearly indicates an increase in deflection over time due to charge migration. The presence of a second polysilicon electrode, as in the device of Fig. 4, eliminates the charge migration effect because the second electrode holds the lower boundary of the gap at a fixed, known potential.

Note that as a surface leakage effect, charge migration will be extremely sensitive to humidity and temperature and may not be consistently reproducible. Similarly, the charging time constant may vary over a wide range of values. The plot of Fig. 13, for example, shows the deflection versus time with 37 V applied to a different actuator having a much shorter measured charge-migration time constant. In this case, the field enhancement due to charge migration causes the actuator to reach snap-through instability. Contact between the membrane and the nitride layer removes the charge on the nitride surface, restoring the actuator to its original condition. The result is a deflection which oscillates in time with period determined by the charge-migration time constant.

## 6. CONTACT CHARGING EFFECT

When the actuator of Fig. 3 reaches snap through, the polysilicon membrane makes contact with the insulating nitride layer that covers the silicon substrate. Contact between these dissimilar materials can result in triboelectric charging, causing residual charge to be left on the nitride surface after the voltage is reduced and membrane contact ceases. When the contact charge on the nitride layer is of the same polarity as the energized membrane, membrane deflection per unit voltage is reduced. Charge deposited by contact will eventually relax to ground over leakage paths on a time scale comparable to the charge-migration time constant described earlier. The plot of Fig. 14 illustrates the contact charging effect. An actuator of the type shown in Fig. 3 having a snap-through voltage of about 55 V was initially energized to 40 V. After 20 seconds, the voltage was increased above snap through for 10 seconds to produce membrane-to-nitride contact, then returned to the initial value of 40 V. As shown in the figure, deflection just after snap through is reduced by about 15%. An analysis based on Eqs. (1) - (4) provides an estimate of the contact charge density. With charge density $\rho_s$ on the nitride surface, the boundary condition (4) becomes

$$\epsilon_0 E_1{}^* = \epsilon_2 E_2 - \rho_s \tag{7}$$

where $E_1{}^*$ is the charge-modified gap field. Solving Eqs. (3) and (7) yields

$$E_1{}^* = \frac{\epsilon_2(V/d_2) - \rho_s}{\epsilon_0 + \epsilon_2(d_1/d_2)} \tag{8}$$

The charge density for the actuator of Fig. 12 can be estimated by combining Eq. (8) with the charge-free gap field expression (5) and solving for $\rho_s$:

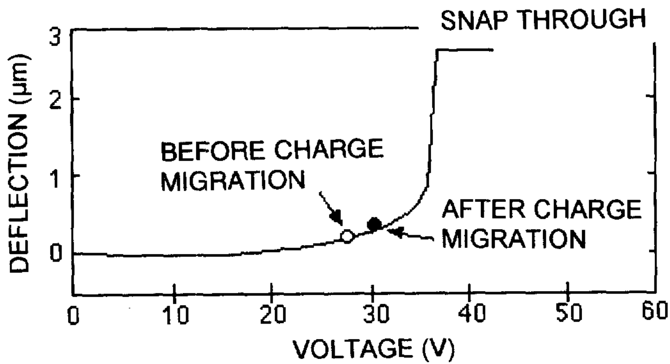


Figure 12 - Measured voltage-deflection curve before charge migration for the actuator used to obtain the plot of Fig. 10. The circles represent the measured deflections obtained from the beginning and ending values in Fig. 10.

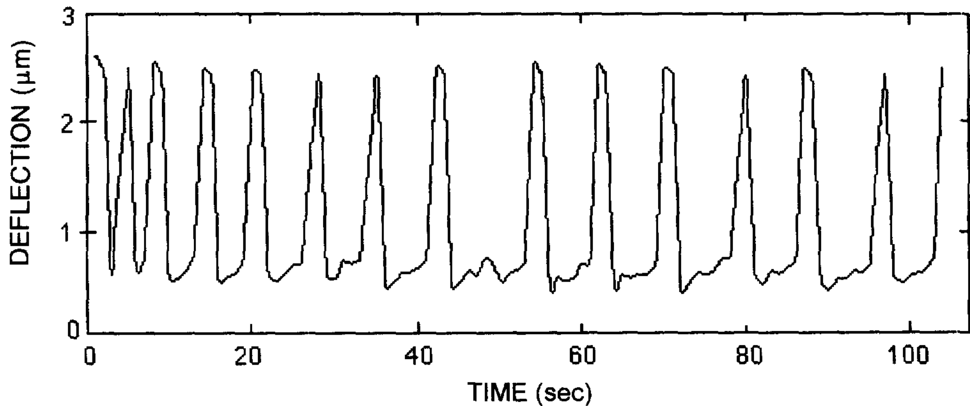


Figure 13 - Deflection versus time for an actuator with a short charge migration time constant. A voltage of 37 V magnitude is applied. For this higher voltage, the charge migration effect causes the device to reach snap-through, an event which discharges the accumulated surface charge.

$$\rho_s = \left(1 - \frac{E_1^*}{E_1}\right)\frac{V}{d_2}\,\epsilon_2 \tag{9}$$

Using the plot of Fig. 12 as a reference, a 15% reduction in deflection just below snap through translates to about a 10% reduction in the gap field, yielding a field ratio $E_1^*/E_1$ of 0.9. Substituting $E_1^*/E_1 = 0.9$ into Eq. (9) with $V = 40$ V and $d_2 = 0.5$ $\mu$m yields $\rho_s \approx 1.4 \times 10^{-4}$ C/m$^2$. Note that the actuator structure of Fig. 4, with its additional polysilicon electrode, reduces the contact charging effect because tribocharging between similar materials is likely to result in much smaller amounts of surface charge. Also, any contact charge that is produced is quickly conducted away by the electrodes, restoring the system to its pre-contact condition.

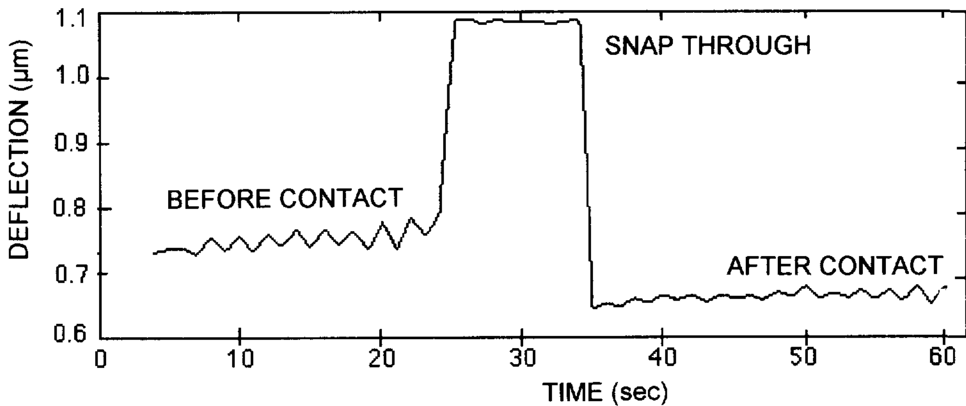


Figure 14 - Actuator deflection before and after a snap-through contact event. Residual charge on the nitride layer initially reduces the deflection of the actuator.

## 7. CONCLUSION

The characteristics of individual double cantilevered polysilicon MEMS actuator cells have been evaluated for possible use in large-scale deformable mirror arrays. Observed actuator characteristics, including the basic form of the deflection vs. voltage curve, can be explained by way of simple electrostatic models. While immune to catastrophic short circuits and likely to lead to more robust systems, actuators with only an insulating layer beneath the membrane exhibit undesirable charge migration and contact charging effects which can be eliminated by using a second polysilicon electrode at the lower end of the gap.

## 8. REFERENCES

1. J.D. Cobine, *Gaseous Conductors,* New York: Dover Press, 1958.

2. R.M. Schaffert, *Electrophotography,* New York: John Wiley, 1975, pp. 514.

3. J.M. Crowley, "Dimensionless Ratios in Electrohydrodynamics", in *Handbook of Electrostatic Processes,* J.S. Chang, A.J. Kelly, J.M. Crowley, eds. New York: Marcel Dekker, Inc., 1995, p. 101.

4. P. Osterberg, H.Yie, X. Cai, J. White, S. Senturia, "Self Consistent Simulation and Modeling of Electrostatically Deformed Diaphragms", *Proc. MEMS '94,* Oiso, Japan, Jan '94

5. J. R. Gilbert, R. Legtenberg, and S.D. Senturia, "3-D Coupled Electromechanics for MEMS: Applications of CoSolve-EM," *Proceedings MEMS '95,* Amsterdam, July 1995.

6. D. Maier-Schneider, J. Maibach, E. Obermeier, "A New Analytical Solution for the Load Deflection of Square Membranes", *Jour. Microelectromechanical Systems,* 4 (4), Dec. 1995.

7. M.A. Michalicek, V.M Bright, and J.H. Comtois, "Design, Fabrication, Modeling, and Testing of a Surface-Micromachined Micromirror Device", *Proc. of the ASME: Dynamic Systems and Control Division,* DSC 57-2,1995.